Applied Catalysis B: Environmental 108–109 (2011) 47–53

Contents lists available at ScienceDirect

Applied Catalysis B: Environmental

journal homepage: www.elsevier.com/locate/apcatb

Visible light photocatalytic activity enhancement for water purification in Cu(II)-grafted WO_3 thin films grown by photoreaction of nanoparticles

Tomohiko Nakajima*, Takuya Kitamura, Tetsuo Tsuchiya

National Institute of Advanced Industrial Science and Technology, Tsukuba Central 5, 1-1-1 Higashi, Tsukuba, Ibaraki 305-8565, Japan

ARTICLE INFO

Article history:
Received 26 May 2011
Received in revised form 2 August 2011
Accepted 5 August 2011
Available online 16 August 2011

Keywords:
WO_3
Photocatalyst
Nanoparticles
Laser treatment
Water purification

ABSTRACT

We have developed a simple process for improving the visible light photocatalytic activity in Cu(II)-grafted WO_3 thin films, called 'the photoreaction of nanoparticles' (PRNP). The films prepared by PRNP showed an enhanced photodegradation rate for an organic dye. Glass substrates were coated with WO_3 nanoparticles (5–30 nm) obtained by wet ball milling, and a post-treatment of either conventional heating or PRNP using KrF laser irradiation was carried out. Compared with the conventional heat treatment at 500 °C, PRNP significantly enhanced surface crystallite growth; pulsed photothermal gradient heating and photochemical stimulation increased the formation of new bonds between nanoparticles. The crystallite size near the surface of the WO_3 film after 7500 pulses of laser irradiation increased to 70 nm, while it was largely-unchanged in the sample prepared by heat treatment at 500 °C. The photocatalytic dye degradation under visible light irradiation was measured for the samples after Cu(II)-grafting, and showed that the degradation rate of the sample prepared by the PRNP process was 2.8-fold higher than that of the sample prepared by heating at 500 °C. We propose that the improved surface crystallinity of WO_3 thin films after the PRNP process stimulates the photoexcited electron/hole transfer at the film surface, resulting in the enhancement of photocatalytic activity.

1. Introduction

The development of simple, efficient water purification is a pressing global issue for environmental protection and to ensure the supply of clean drinking water [1,2]. The huge tsunami on the northeast Japanese coast in March 2011 caused the breakdown of many water treatment plants which use microbial treatment, and highlighted the difficulty in quickly restoring their function [3]. Simple, robust water treatment equipment is therefore necessary as an emergency backup system. An inorganic photocatalyst water treatment system which uses sunlight or ultraviolet lamp irradiation would be suitable for emergencies or for routine purification in terms of the ease of manageability if the catalytic activity in such devices is sufficiently improved [4–7].

WO_3, an n-type semiconductor with band gap energy of 2.8 eV, is well known as a visible light photocatalyst, and has been already used for solar energy conversion [8–11]. Recently, the photodegradation properties of WO_3 have been improved by modifications such as metal adsorption and the surface grafting of transition metal ions [12–14]. Irie et al. have demonstrated a significant enhancement in visible light photocatalytic oxidation by grafting Cu(II) onto the surface of WO_3 [14]. They suggested the effects of Cu(II)-grafting at the catalyst surface as follows: (1) a multi-electron oxygen reduction induced by the grafted Cu(II) ions enhanced the decomposition of organic compounds under visible light excitation; and (2) a visible light absorption was enhanced.

Because of their facile fabrication process, the photocatalysts commonly used in practical applications are heat-treated photocatalytic nanoparticle coating films. We have recently investigated a new process using the photoreaction of nanoparticles (PRNP) [15], where a nanoparticle-coated film was irradiated with an excimer laser, and was found to significantly promote crystal growth at very low temperatures. We have also studied how oxide materials grow under excimer laser irradiation; crystal nuclei in the precursor matrix absorbed the laser light and the crystal grain growth was enhanced by photochemical and photothermal effects [16,17]. Low temperature crystal grain growth is very useful for various types of material; therefore it should also be effective for photocatalytic coated materials. We herein report the application of the PRNP to photocatalytic WO_3 films, and the effect of laser irradiation on the photocatalytic activity compared with films prepared by conventional heat treatment.

2. Experimental

WO_3 nanoparticles were obtained by wet ball milling (Planet-M, Nagao System Inc.) using WO_3 powder (Rare Metallic Inc.) in alcohol solution. The composition of the reagent WO_3 powder was

* Corresponding author.
E-mail address: t-nakajima@aist.go.jp (T. Nakajima).

0926-3373/$ – see front matter © 2011 Elsevier B.V. All rights reserved.
doi:10.1016/j.apcatb.2011.08.006

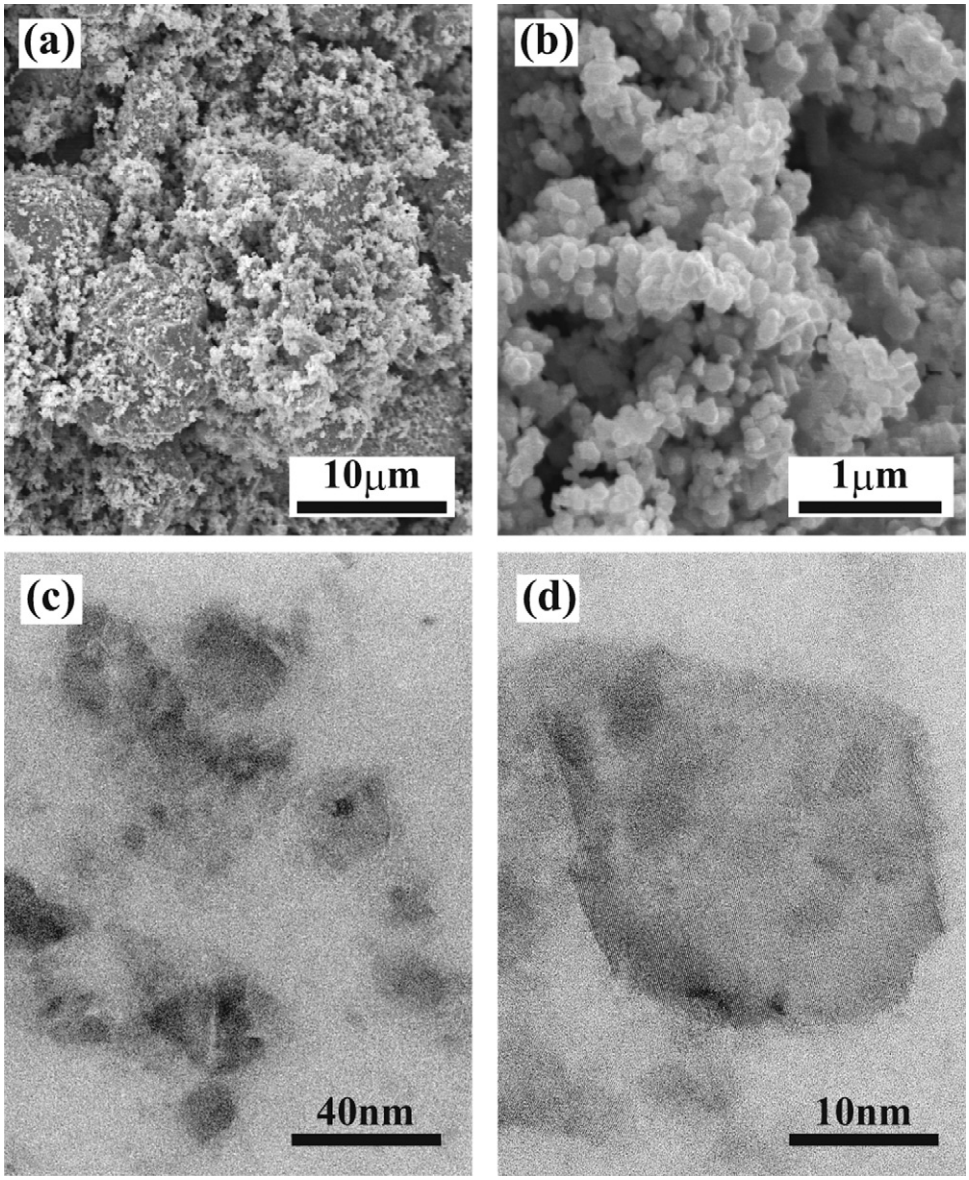

Fig. 1. (a, b) SEM images for the WO_3 reagent powder and (c, d) the TEM images for WO_3 nanoparticles obtained by the ball milling of reagent powder.

confirmed to be granular, comprising submicrometer small particles and fixed large grains 10 μm in size, as shown in the field emission scanning electron microscope (FESEM) images (Fig. 1(a) and (b)). The milled dispersion was filtered to remove the coarse particles, and the particle size in the final solution was evaluated as 5–30 nm, as shown in the transmission electron microscope (TEM) images (Fig. 1(c) and (d)). The dispersion was spin-coated onto borosilicate glass substrates (Corning 1737) at 3000 rpm for 10 s. Silica glass substrates were used in the samples for UV–Vis transmission spectroscopy measurements. The coated films were dried at 100 °C in air for 10 min, and the spin coating and preheating sequence was repeated three times to increase the film thickness. The film was confirmed to be 120 nm thick by cross-sectional transmission electron microscopy (XTEM).

The WO_3 nanoparticle-coated films were subjected to post-treatments of either conventional heating or excimer laser irradiation. Heat treatment consisted of heating the coated samples in a box furnace at 100 °C or 500 °C in air for 60 min. In the PRNP process, the coated films were irradiated by a KrF laser (Compex110, Lambda Physik; pulse duration: 26 ns) at a fluence of 50 mJ/cm^2 for 300–7500 pulses in air at room temperature.

The crystal structure of the prepared films was determined by X-ray diffraction analysis (SmartLab, Rigaku). The FESEM and TEM analyses were carried out using S-800 (Hitachi Ltd.) and H9000 (Hitachi Ltd.) instruments, respectively. The absorbance spectra of the films were recorded by UV–Vis transmission spectroscopy and the surface morphology was observed by atomic force microscopy (AFM). Temperature variations during excimer laser irradiation was simulated using the heat diffusion equation simplified for one-dimensional heat flow, as previously reported in the literature [16,18]. Previously published physical constants for WO_3 and the borosilicate substrate were used in the simulation [19–21]. For the relative comparison of the photocatalytic activity of the films, the photodecomposition of methylene blue (MB) ($C_{16}H_{18}ClN_3S{\cdot}3H_2O$, Merck Chemicals) in water with an initial concentration of 1.5×10^{-5} mol/L was measured. Cu(II) was grafted onto the WO_3 film surface by impregnation with an aqueous solution of $CuCl_2{\cdot}2H_2O$ at 90 °C for 60 min before the photocatalytic

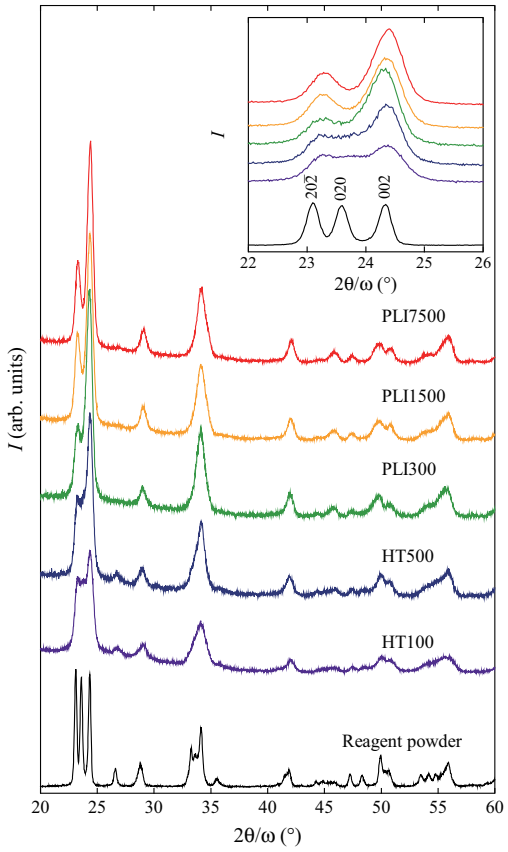

Fig. 2. The $2\theta/\omega$ X-ray diffraction patterns for the WO_3 reagent powder and thin films on glass substrates obtained by heat treatment (HT100 and HT500) and PRNP (PLI300, PLI1500 and PLI7500). The inset shows the enlarged profiles around the $2\ 0\ \bar{2}$, 0 2 0 and 0 0 2 diffraction peaks for the samples.

tests. The Cu(II)-grafted WO_3 (Cu/WO_3) films (15 mm × 15 mm) were immersed in the dye solution (80 mL). The absorbance of MB at 664 nm was measured with a UV–Vis spectrometer to track the photodegradation of MB as a function of time under homogenized visible light (15 mm × 10 mm, 100 kLux, Xe lamp, 300 W) through a UV cut-off filter ($\lambda < 400$ nm).

3. Results and discussion

3.1. X-ray structural analysis

The crystal growth of the samples prepared by heat treatment at 100 °C (HT100) and 500 °C (HT500) and the samples prepared by pulsed laser irradiation for 300 pulses (PLI300), 1500 pulses (PLI1500) and 7500 pulses (PLI7500) were compared using X-ray diffraction. Fig. 2 shows the X-ray $2\theta/\omega$ scans for the samples and the WO_3 reagent powder. The reagent WO_3 powder showed monoclinic diffraction patterns with a unit cell of $a = 0.7306$ nm, $b = 0.7540$ nm, $c = 0.7692$ nm, and $\beta = 90.881°$ [22]. The peak shape of the reagent powder was significantly broader than that of the HT100 sample because of surface damage from the ball milling process and the nano-size effect. In the HT500 sample, the diffraction peaks were larger and a weak 0 0 1 orientation was observed. In the samples prepared by the PRNP process, the PLI300 sample exhibited significantly enhanced crystal growth and an increase in the 0 0 1 orientation. The crystal growth and the 0 0 1 orientation increased as the number of laser pulses applied to the sample increased compared with the conventional heat treated samples.

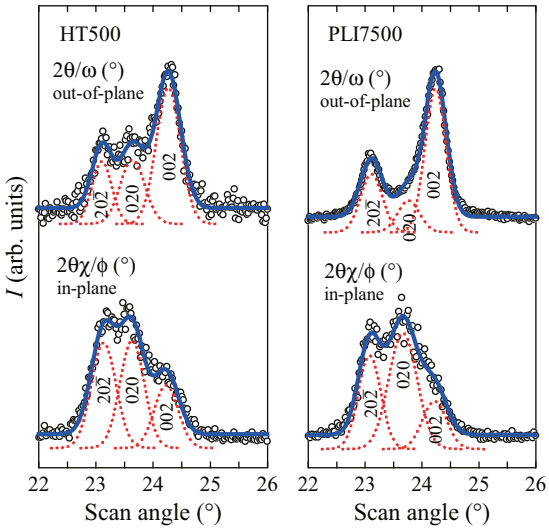

Fig. 3. The $2\theta/\omega$ and $2\theta\chi/\phi$ X-ray diffraction profiles for the HT500 and PLI7500 samples around the $2\ 0\ \bar{2}$, 0 2 0 and 0 0 2 diffraction peaks. The circles are observed data, and the blue solid and red dotted lines represent the fitted lines and the calculated Gaussian peaks, respectively. (For interpretation of the references to color in this figure legend, the reader is referred to the web version of the article.)

The X-ray diffraction profiles for the selected angle around the $2\ 0\ \bar{2}$, 0 2 0 and 0 0 2 indices of the $2\theta/\omega$ (out-of-plane) and $2\theta\chi/\phi$ (in-plane) scans are shown in Fig. 3. In the HT500 sample, the 0 0 2 peak increased in the out-of-plane profile and decreased in the in-plane profiles, whereas the intensity ratio of $2\ 0\ \bar{2}$/0 2 0 was largely unchanged compared with the unoriented reagent powder. However, the 0 0 2 peak was stronger and the 0 2 0 peak was weaker compared with the $2\ 0\ \bar{2}$ peak intensity in the out-of-plane profile for the PLI7500 sample. In the in-plane profile, the intensity ratios of $2\ 0\ \bar{2}$/0 2 0 and 0 0 2/0 2 0 increased by 24% and decreased by 36%, respectively, compared to those for HT500. These variations in peak intensities indicate the anomalous preferred orientation where the deposited incidentally (0 1 0)-oriented domain was selectively converted to the (0 0 1)-oriented domain by pulsed laser irradiation.

The average crystallite size D for each sample was calculated using Scherrer's equation [23], $D = (K \cdot \lambda / \beta \cos\theta)$, where K is the Scherrer constant ($K = 0.94$), λ is the wavelength of the incident X-ray ($\lambda = 0.15401$ nm), β is the full width at half-maximum intensity of the 0 0 2 peak, and θ is the Bragg diffraction angle ($2\theta = 24.25°$). Fig. 4 shows the calculated average crystallite size D and the out-

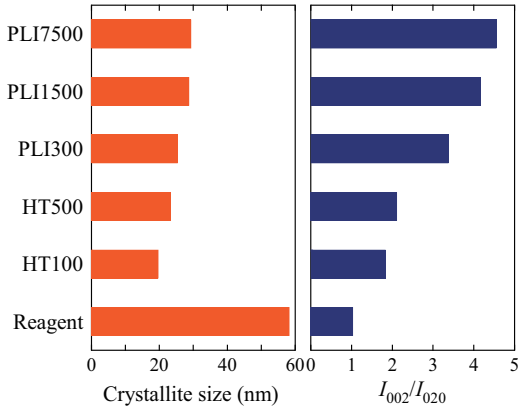

Fig. 4. Calculated crystallite size and X-ray diffraction peak ratio (I_{002}/I_{020}) for the WO_3 reagent powder and thin films obtained by heat treatment (HT100 and HT500) and PRNP (PLI300, PLI1500 and PLI7500).

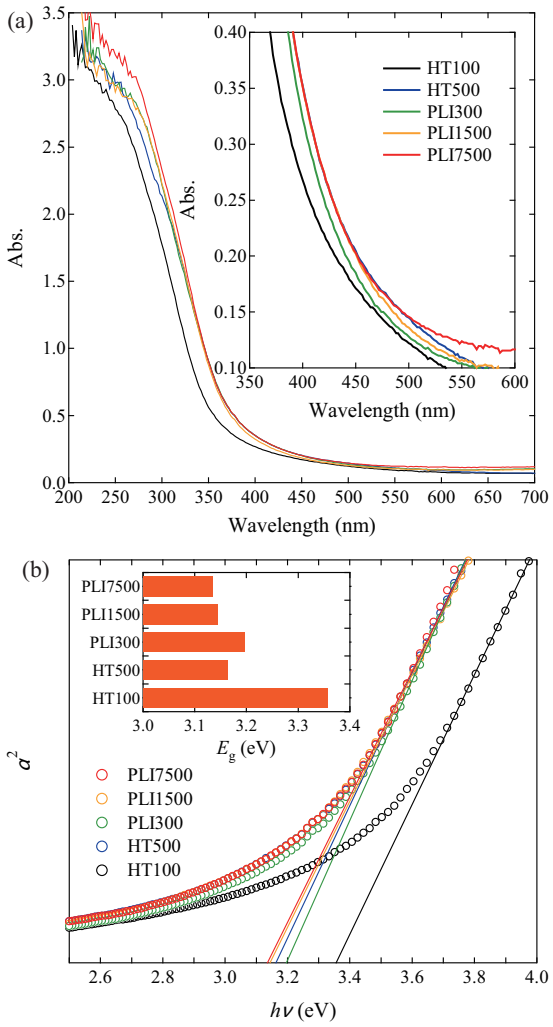

Fig. 5. (a) The optical absorbance for the samples of WO_3 thin films, and (b) the α^2–$h\nu$ plot for the samples. The inset shows the band gap energy.

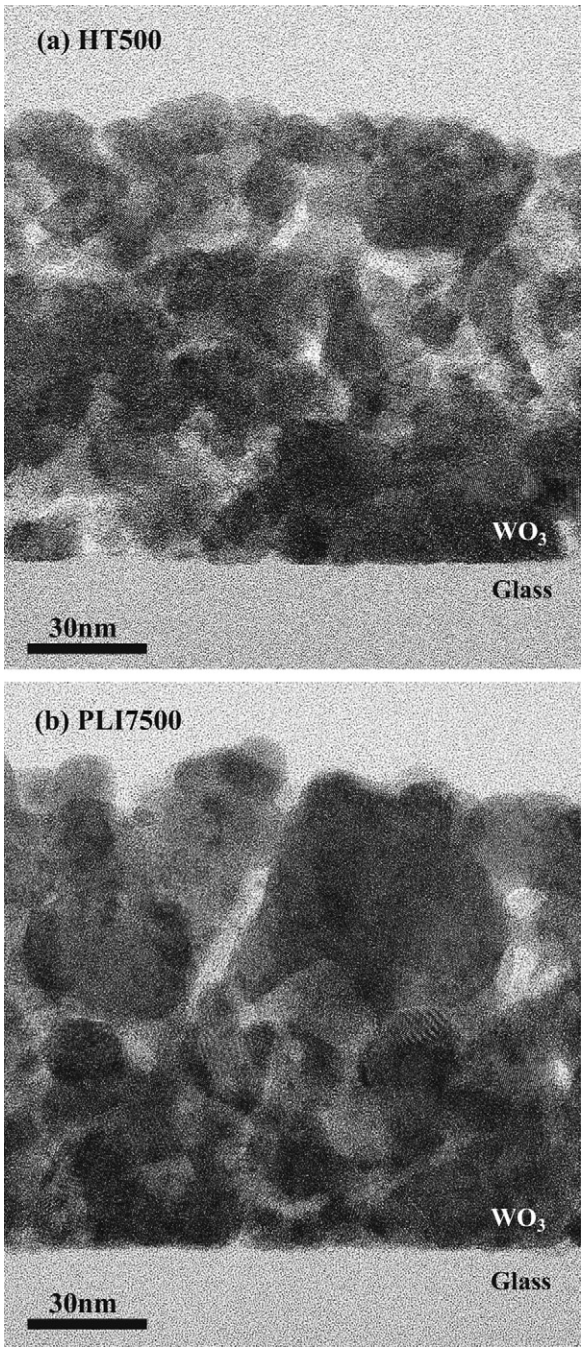

Fig. 6. XTEM images of the WO_3 thin films on glass substrates obtained by (a) heat treatment (HT500) and (b) PRNP (PLI7500).

of-plane X-ray diffraction peak intensity ratio I_{002}/I_{020} for the WO_3 reagent powder and the films prepared by heating and PRNP. The average crystallite size of WO_3 in the HT100 sample, where the nanoparticle dispersion was dried onto the substrate, dropped by one-third (D = 19.8 nm) compared to that of the reagent powder (D = 58.3 nm) because of particle fracturing from ball milling. In contrast, heat treatment at 500 °C allowed the crystallites grow to 23.3 nm in the HT500 sample, and the pulsed laser treatment sample PLI7500 contained crystallites that had grown up to 29.3 nm at room temperature. From the I_{002}/I_{020} variation, the strong 0 0 1 orientation with the number of laser pulses compared with the heat treatment samples was revealed. Thus, it was confirmed that the WO_3 films exhibited anomalous crystallite growth which cannot be achieved by conventional heat treatment.

3.2. Optical properties

The UV–Vis absorbance spectra and α^2–$h\nu$ plot (α, absorption coefficient) for the samples obtained by heat treatment and PRNP are shown in Fig. 5. The optical band gap energy (E_g) of the HT100 sample, estimated from the absorption edge, was significantly blue-shifted to E_g = 3.36 eV from the literature value (E_g = 2.8 eV) of bulk WO_3 powder [8–11]. This can be explained by the nano-size effect [24] in combination with a surface amorphous effect [25] caused by mechanical milling damage. The TEM image in Fig. 1(c) shows the presence of both angular nanocrystals and indistinct edge amorphous grains. The blue-shift disappeared after crystal reformation during the heat treatment process at 500 °C. The E_g of the HT500 sample decreased to 3.16 eV, although the value was still larger than that of bulk sample because of the nano-size effect from the small crystallite size (D = 23.3 nm) and the thin film thickness (120 nm). A similar decrease in E_g was observed in the samples prepared by the PRNP process. As the laser pulse number increased, the E_g of the samples was decreased from 3.20 eV (PLI300) to 3.13 eV (PLI7500) as the size of the crystallites increased (Fig. 4). The values of E_g for the samples heated at 500 °C and the PRNP samples were similar to the reported value for WO_3 thin films [26], indicating the absorbance of visible light (λ > 400 nm).

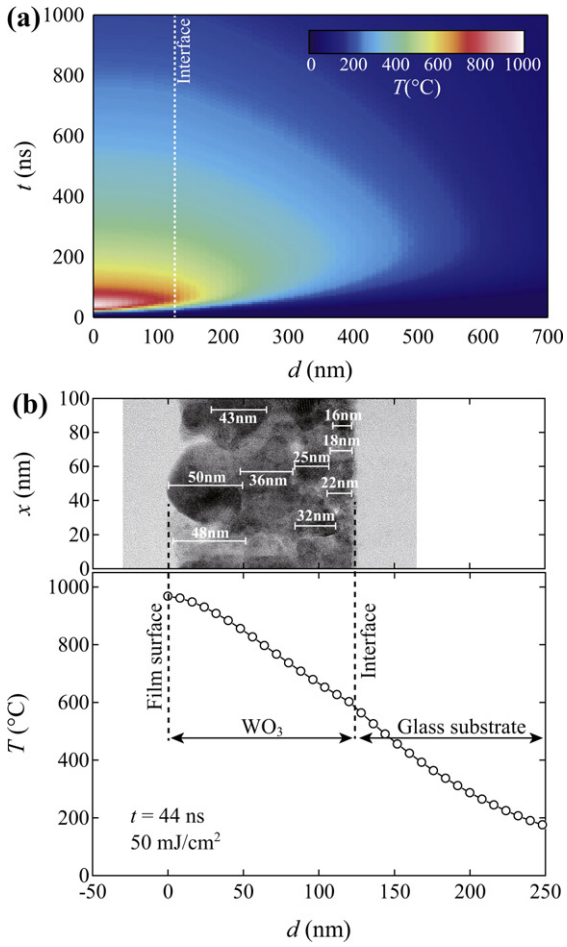

Fig. 7. (a) Simulated temperature map for depth (d) and time (t) dependences in the WO_3/glass under KrF laser irradiation at a fluence of 50 mJ/cm^2. The initial substrate temperature was fixed at 20 °C. (b) The relationship between the crystalline structure of the WO_3 thin film PLI7500, shown by the XTEM image and the depth dependence of temperature variation with a fluence of 50 mJ/cm^2 at 44 ns after the incident pulse.

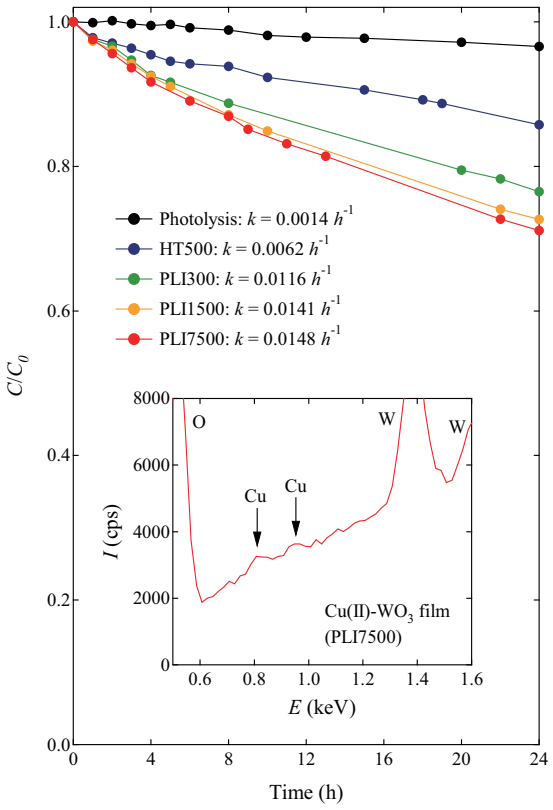

Fig. 8. The photocatalytic degradation of MB for the HT500, PLI300, PLI1500 and PLI7500 samples, after Cu(II)-grafting post treatment, under visible light irradiation, reported as the ratio of the dye concentration and the initial concentration (C/C_0). The photolysis of MB is also plotted as a blank measurement. The inset shows the energy dispersive X-ray spectrum for the Cu(II)-grafted WO_3 film derived from the PLI7500.

3.3. *Microscopic structural analysis and anomalous crystallite growth during the PRNP process*

The XTEM images for the HT500 and PLI7500 samples were used to examine the microscopic structure (Fig. 6). In the HT500 sample, the 5–30 nm WO_3 nanocrystalline particles similar to the initially deposited particles were observed in the film; the crystallite size was consistent with the calculated value from the X-ray diffraction data (Fig. 4). The particle size distribution in the film was random. In contrast, the particle size distribution for the film prepared by laser irradiation (PLI7500) showed a gradient particle size distribution. The crystallites near the film surface were significantly larger, up to 70 nm, and their size gradually decreased as the depth increased (Fig. 5(b)). The crystallite size near the film/substrate interface (5–30 nm) was similar to that of the HT500 sample. X-ray diffraction analysis of the crystallite size showed that D for the PLI7500 sample was 29.3 nm. However, XTEM analysis confirmed that the calculated crystallite size of the laser irradiated samples from the X-ray diffraction was an average value for the whole film, and did not take into account the particle size distribution gradient. This anomalous grain growth in the WO_3 film is a novel feature of the PRNP process.

Fig. 7(a) shows the simulated temperature distribution for a WO_3 film on a borosilicate substrate under KrF laser irradiation at a fluence of 50 mJ/cm^2. The temperature rapidly increases to 967 °C from photothermal heating at the WO_3 film surface, 44 ns after the incident pulse. The depth profile of the temperature variation exhibits a gradient in the temperature, decreasing from the film surface to the substrate. The photothermal heating drops below 500 °C after 200 ns. The XTEM image for a selected part of the PLI7500 sample and the depth dependence of the photothermal temperature variation (t = 44 ns) are shown in Fig. 7(b). The gradient temperature varies from 967 °C at the film surface to 602 °C at the interface, leading to the enhanced crystallite growth at the film surface. However, this phenomenon cannot be explained by photothermal heating alone. The enhanced crystallite growth occurred well below the melting point of WO_3 (1473 °C) [27]. This indicates that the growth mechanism is independent of melt growth, such as that seen in the laser annealing process for polysilicon formation [28,29], and there would be the other strong driving force for the rapid fusing of the nanoparticle grains. We have previously investigated the presence of strong photochemically activated crystallization at the reaction interface during the process of oxide film growth by pulsed laser irradiation. A photochemically activated dangling bond on a grain surface could form new chemical bonds with neighboring activated bonds [16,17]. For polycrystalline growth in Dion-Jacobson type perovskite oxides, we have previously confirmed large, in-plane grain growth of several micrometers under KrF laser irradiation, with a strong preferred orientation induced by the large gradient temperature variation from the film surface [30,31]. This was also achieved by photochemical activation at the growth interface. Thus, we can conclude that the anomalous crystallite growth of WO_3 in this study was induced by both the photothermal pulsed heating and the photochemically activated WO_3 nanoparticle surface.

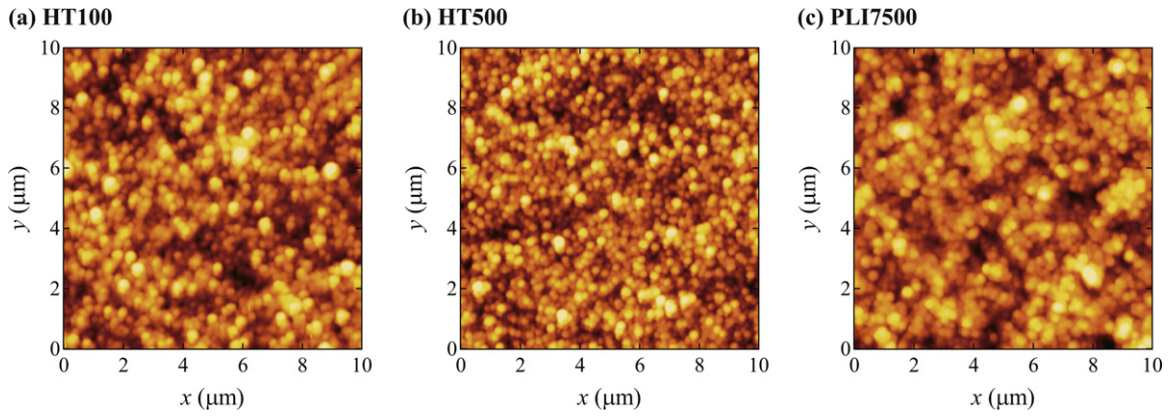

Fig. 9. The surface morphology observed by AFM in a 10 μm × 10 μm region for (a) HT100, (b) HT500 and (c) PLI7500.

3.4. Photocatalytic activity for water purification and practical applications of PRNP

The photocatalytic degradation of MB under visible light irradiation achieved by the HT500, PLI300, PLI1500 and PLI7500 samples after further treatment by Cu(II)-grafting, was measured as the ratio of the final and the initial dye concentration (C/C_0) (Fig. 8). (The Cu(II)-grafted films were successfully obtained by impregnation using $CuCl_2{\cdot}2H_2O$. From the energy dispersive X-ray analysis, the Cu was clearly observed at film surface in the spectrum as shown in the inset of Fig. 8, while the Cl ions were never detected. The Cu content was evaluated to be 0.47 at%. This grafting property was consistent with the previous report by Irie et al. [32]. The samples prepared by the heating and PRNP processes both exhibited photocatalytic activity, and the MB dye decomposed further as the exposure to visible light increased. In order to compare the photocatalytic activity, first-order decomposition kinetics were used; $\ln(C/C_0) = kt$, where k is a kinetic constant and t is visible light illumination time. The value of k for the HT500 sample was calculated as $6.2 \times 10^{-3}\ h^{-1}$, in the PLI300 sample, the value jumped to $1.16 \times 10^{-2}\ h^{-1}$, and in the PLI7500 sample the value reached $1.48 \times 10^{-2}\ h^{-1}$. The real kinetic constant for the PLI7500 sample was estimated to be 2.8-fold larger than that for the HT500 sample, when the blank photolysis rate constant was taken into account. In photocatalytic reactions, photoexcited electron/hole transfers are significant in the oxidation of dye molecules and the reduction of oxygen at the film surface [33–35]. The surface crystallinity, which depends on sufficient crystallite growth in WO_3 thin films, was greatly improved by pulsed laser irradiation in the PRNP process. The enhanced crystallinity should therefore stimulate the photoexcited electron/hole transfer at the film surface, resulting in the improvement of the photocatalytic activity.

Fig. 9 shows AFM images of the surface morphology of a 10 μm × 10 μm region of the HT100, HT500 and PLI7500 samples. The sample where the deposited WO_3 nanoparticles were dried at 100 °C (HT100) had a submicrometer scale granular surface morphology with $Ra = 16.3$ nm and $S = 1.023 \times 10^2\ \mu m^2$, where the Ra is the surface roughness and the S is the calculated surface area. After heat treatment at 500 °C (HT500), the Ra was reduced to 10.2 nm by moderate sintering of the nanoparticles, and the surface area was reduced to $1.015 \times 10^2\ \mu m^2$. While there was no obvious morphological change in the film surface of the PLI7500 sample compared to the HT500 sample, the Ra and S for the PLI7500 sample decreased to 9.6 nm and $1.004 \times 10^2\ \mu m^2$, respectively, because of further crystallite growth near the surface. This reduction in surface area during the PRNP process indicates that the enhanced photocatalytic activity was not caused by surface morphology, but by other factors, such as the stimulated photoexcited carrier transfer at the film surface arising from the anomalous crystallite growth under pulsed laser irradiation.

Because the PRNP process does not cause morphological changes in the photocatalytic surface, it is suitable for use as a post-treatment to improve the surface crystallinity of photocatalytic materials which have various kinds of surface morphology. For example, the surface crystallinity of mesoporous materials can be significantly improved by pulsed laser irradiation post-treatment without destroying the controlled surface structure. Pulsed laser irradiation post-treatments such as the PRNP process have the potential to become a key technology for improving the photocatalytic activity of various inorganic photocatalysts used in water purification.

4. Conclusions

We have developed a simple new process for enhancing the degradation of organic dye by visible light photocatalysis using Cu(II)-grafted WO_3 thin films. WO_3 nanoparticles were coated onto glass substrates, and the films were either treated with conventional heating or by PRNP using KrF laser irradiation. Compared with the conventional heat treatment at 500 °C, the KrF laser irradiation significantly enhanced the surface crystallite growth. The pulsed photothermal gradient heating and photochemical stimulation allowed the crystallite size near the surface of the WO_3 film exposed to 7500 laser pulses to reach 70 nm, however the sample prepared by heat treatment at 500 °C did not show any significant change in particle size. The photocatalytic degradation of MB under visible light irradiation for the samples after Cu(II)-grafting, showed that the degradation rate for the samples prepared by PRNP was 2.8-fold greater than that of the sample prepared by heating at 500 °C. We propose that the improved surface crystallinity of WO_3 thin films after the PRNP process stimulates the photoexcited electron/hole transfer at the film surface, resulting in the enhancement of photocatalytic activity. PRNP has the potential to be a practical technique for effectively enhancing the activity of a wide variety of inorganic photocatalysts.

Acknowledgements

We are grateful to O. Yoshimi at Suido Kiko Kaisha Ltd. and K. Hatakeyama at Sincere Ltd. for valuable discussions.

References

[1] L. Ahrens, M. Shoeib, T. Harner, S.C. Lee, R. Guo, E.J. Reiner, Environ. Sci. Technol., doi:10.1021/es1036173.
[2] H. Ma, C. Burger, B.S. Hsiao, B. Chu, J. Mater. Chem., doi:10.1039/c0jm04308g.

[3] Press Release from Japanese Ministry of Land, Infrastructure, Transport and Tourism on 15 April, http://www.milt.go.jp/common/000141929.pdf, 2011 (in Japanese).
[4] H. Zhang, G. Chen, D.W. Bahnemann, J. Mater. Chem. 19 (2009) 5089.
[5] C. Sarantopoulos, E. Puzenat, C. Guillard, J.M. Herrmann, A.N. Gleizes, F. Maury, Appl. Catal. B 91 (2009) 225.
[6] Y.-C. Nah, I. Paramasivam, P. Schmuki, ChemPhysChem 11 (2010) 2698.
[7] D.M.A. Alrousan, P.S.M. Dunlop, T.A. McMurray, J.A. Byrne, Water Res. 43 (2009) 47.
[8] M. Butler, J. Appl. Phys. 48 (1977) 1914.
[9] G. Bamwenda, H. Arakawa, Appl. Catal. A 210 (2001) 181.
[10] H. Kominami, K. Yabutani, T. Yamamoto, Y. Kera, B. Ohtani, J. Mater. Chem. 11 (2001) 3222.
[11] S. Berger, H. Tsuchiya, A. Ghicov, P. Schmuki, Appl. Phys. Lett. 88 (2006) 203119.
[12] Z.-G. Zhao, M. Miyauchi, Angew. Chem. Int. Ed. 47 (2008) 7051.
[13] R. Abe, H. Takami, N. Murakami, B. Ohtani, J. Am. Chem. Soc. 130 (2008) 7780.
[14] H. Irie, S. Miura, K. Kamiya, K. Hashimoto, Chem. Phys. Lett. 457 (2008) 202.
[15] T. Tsuchiya, F. Yamaguchi, I. Morimoto, T. Nakajima, T. Kumagai, Appl. Phys. A 99 (2010) 745.
[16] T. Nakajima, T. Tsuchiya, M. Ichihara, H. Nagai, T. Kumagai, Chem. Mater. 20 (2008) 7344.
[17] T. Nakajima, T. Tsuchiya, M. Ichihara, H. Nagai, T. Kumagai, Appl. Phys. Expr. 2 (2009) 023001.
[18] D. Bäuerle, Laser Processing and Chemistry, Springer-Verlag, Berlin, Heidelberg, New York, 2000.
[19] H.T. Wang, Y.B. Xu, M. Goto, Y. Tanaka, M. Yamazaki, A. Kasahara, M. Tosa, Mater. Trans. 47 (2006) 1894.
[20] Y.-F. Gong, Z.-T. Song, Y. Ling, Y. Liu, Y.-J. Li, S.-L. Feng, Chin. Phys. Lett. 27 (2010) 088501.
[21] F. Rao, Z. Song, Y. Gong, L. Wu, B. Liu, S. Feng, B. Chen, Appl. Phys. Lett. 92 (2008) 223507.
[22] B.O. Loopstra, H.M. Rietveld, Acta Crystallogr. B 24 (1982) 1968.
[23] L.V. Azaroff, Elements of X-ray Crystallography, McGrawHill, New York, 1968.
[24] W. Li, J. Li, X. Wang, J. Ma, Q. Chen, Int. J. Hydrogen Energy 35 (2010) 13137.
[25] M. Deepa, R. Sharma, A. Basu, S.A. Agnihotry, Electrochim. Acta 50 (2005) 3545.
[26] K.J. Patel, C.J. Panchal, V.A. Kheraj, M.S. Desai, Mater. Chem. Phys. 114 (2009) 475.
[27] E. Cazzanelli, C. Vinegoni, G. Mariotto, A. Kuzmin, J. Purans, Solid State Ionics 123 (1999) 67.
[28] T. Sameshima, M. Hara, S. Usui, Jpn. J. Appl. Phys. 28 (1989) 1789.
[29] S. Whelan, V. Privitera, M. Italia, G. Mannino, C. Spinella, G. Fortunato, L. Mariucci, M. Stanizzi, A. Mittiga, J. Vac, Technol. Sci. (2002) 644, B20.
[30] T. Nakajima, T. Tsuchiya, T. Kumagai, Cryst. Growth Des. 10 (2010) 4861.
[31] T. Nakajima, T. Tsuchiya, T. Kumagai, CrystEngComm 13 (2011) 158.
[32] H. Irie, K. Kamiya, T. Shibanuma, S. Miura, D.A. Tryk, T. Yokoyama, K. Hashimoto, J. Phys. Chem. C 113 (2009) 10761.
[33] P.V. Kamat, Chem. Rev. 93 (1993) 267.
[34] D.W. Bahnemann, M. Hilgendorff, R. Memming, J. Phys. Chem. B 101 (1997) 4265.
[35] M. Miyauchi, A. Nakajima, T. Watanabe, K. Hashimoto, Chem. Mater. 14 (2002) 4714.